Supporting Information

Nanoscale Characterization of Halide Perovskite Phase Stability with Scanning Electron Microscopy

Jeffrey A. Christians,* Rory Campagna, Ian J. McGovern, Brian Tran

Affiliations:
Department of Engineering, Hope College, Holland, MI 49423, USA

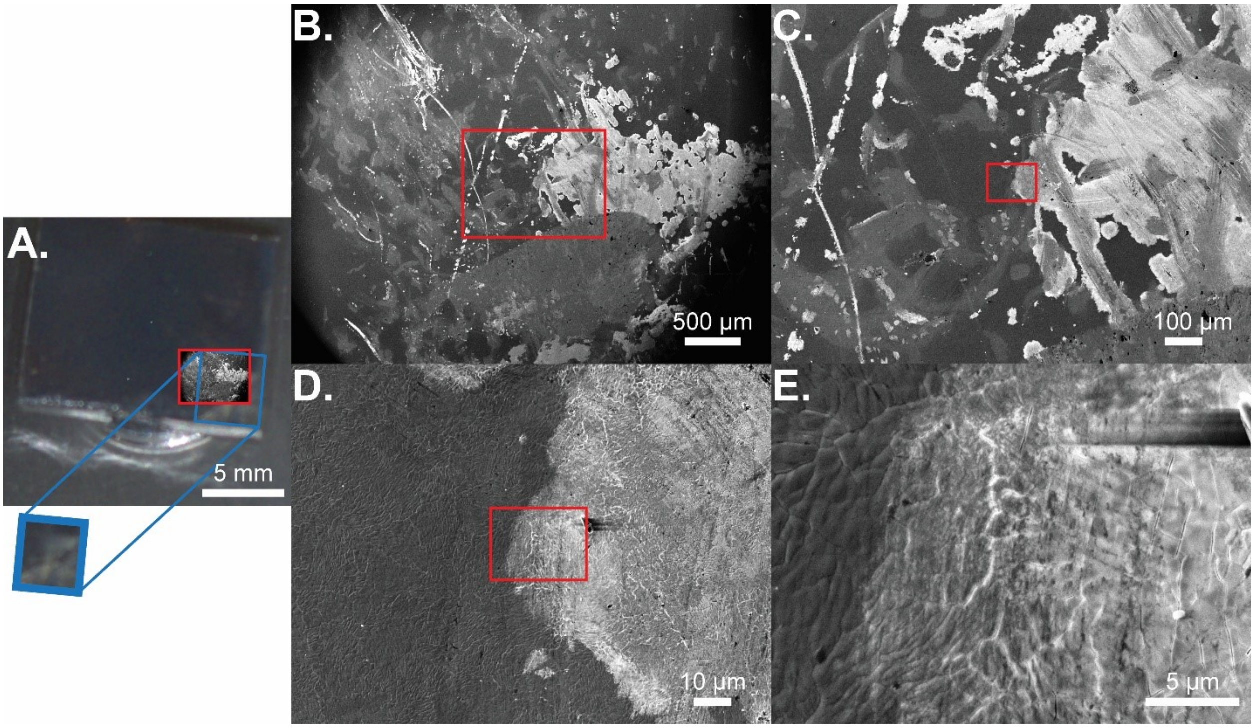

Figure S1. Increasing magnification of the perovskite/non-perovskite interface in a $CsPbI_3$ film. (A) A low-resolution photograph taken inside the scanning electron microscope (SEM). The blue square shows the optical image of a portion of the film with some clear δ-$CsPbI_3$, while the red square is a live scanning electron micrograph of the film. (B) – (D) show SEM images with progressively increasing magnifications of the same location on the $CsPbI_3$ film. The red rectangles in each image correspond to the location of the next, higher magnification image, for example, the red box in (B) corresponds to the full frame image shown in (C).

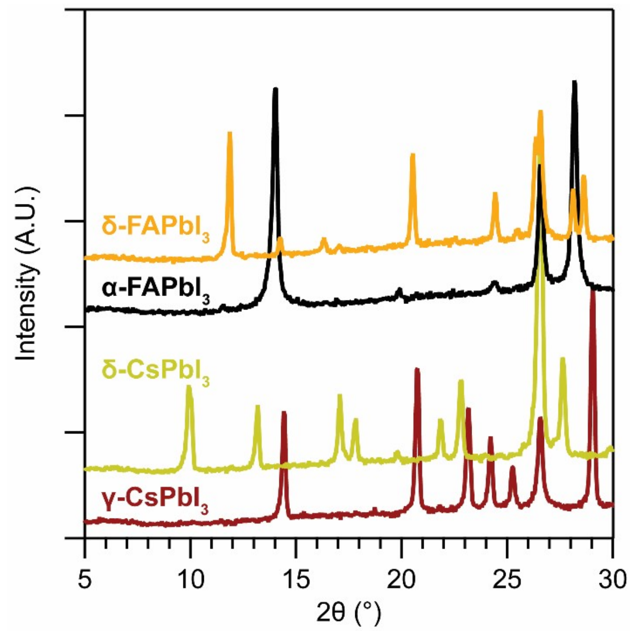

Figure S2. X-ray diffraction patterns of materials. X-ray diffraction patterns shown of the initial materials in their perovskite phases (γ-$CsPbI_3$ and α-$FAPbI_3$) as well as these materials after they have gone through the phase change into the non-perovskite or δ-phase (δ-$CsPbI_3$ and δ-$FAPbI_3$).

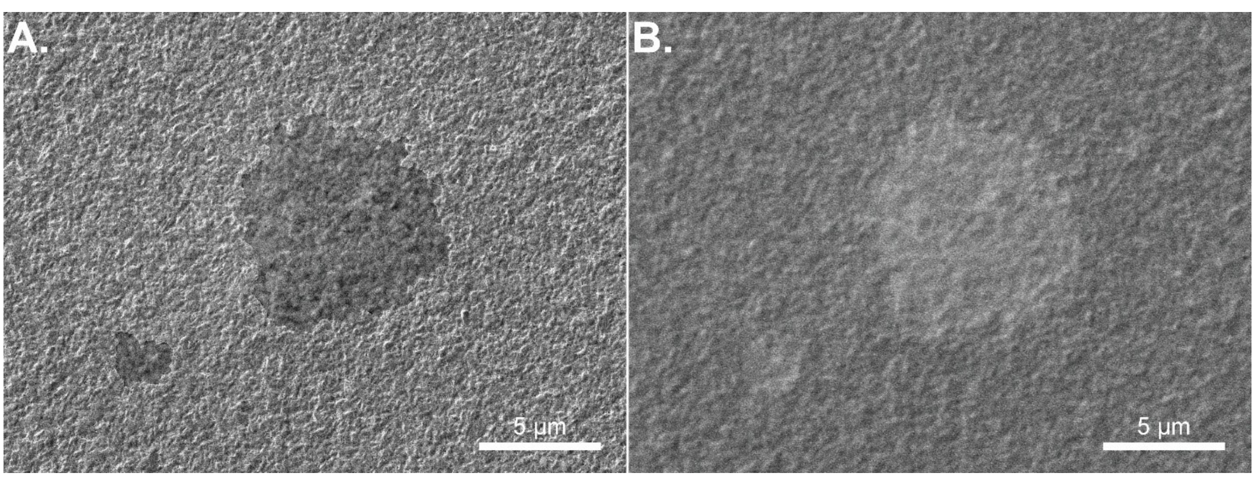

Figure S3. Dwell time and image contrast. An image of δ-$CsPbI_3$ regions imaged with different dwell times. Both images were obtained with a primary beam voltage of 1.7 kV and the probe current set to a value of 30. Image (A) has a dwell time of 16.3 μs while image (B) was obtained by integrating multiple scans while using a dwell time of 0.81 μs.

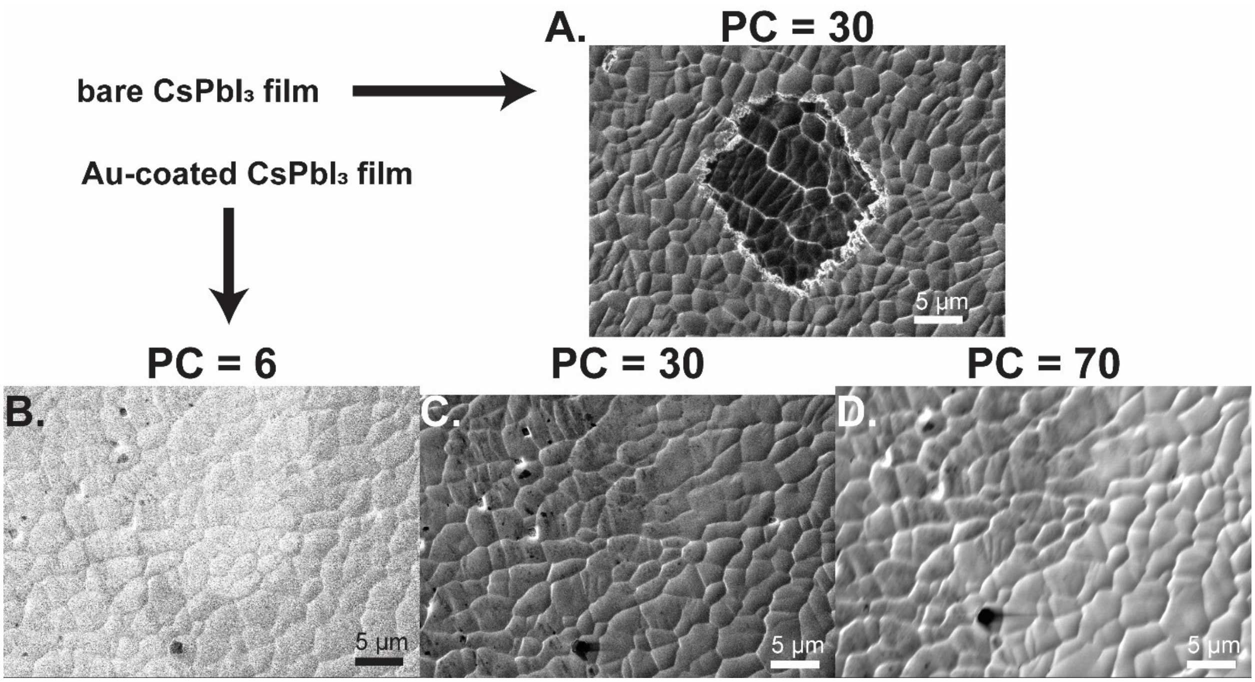

Figure S4. Reduced charging with Au sputter coating. (A) A typical image of a δ-CsPbI3 region in a γ-$CsPbI_3$ film with a probe current setting of 30. The δ-$CsPbI_3$ region appears dark due to positive charging. The images in (B) – (D) show increasing probe current while imaging a $CsPbI_3$ film with a thin Au layer, deposited by sputter coating using an Ar plasma sputter source. Higher electron beam currents are needed to induce positive charging and contrast reversal. The Au film in (D) at PC = 70 taken with 2x exposure time to induce charging. All images were obtained with a primary beam energy of 2.3 kV. The Au coating decreases the overall contrast seen between the two phases because it changes the surface of the film.

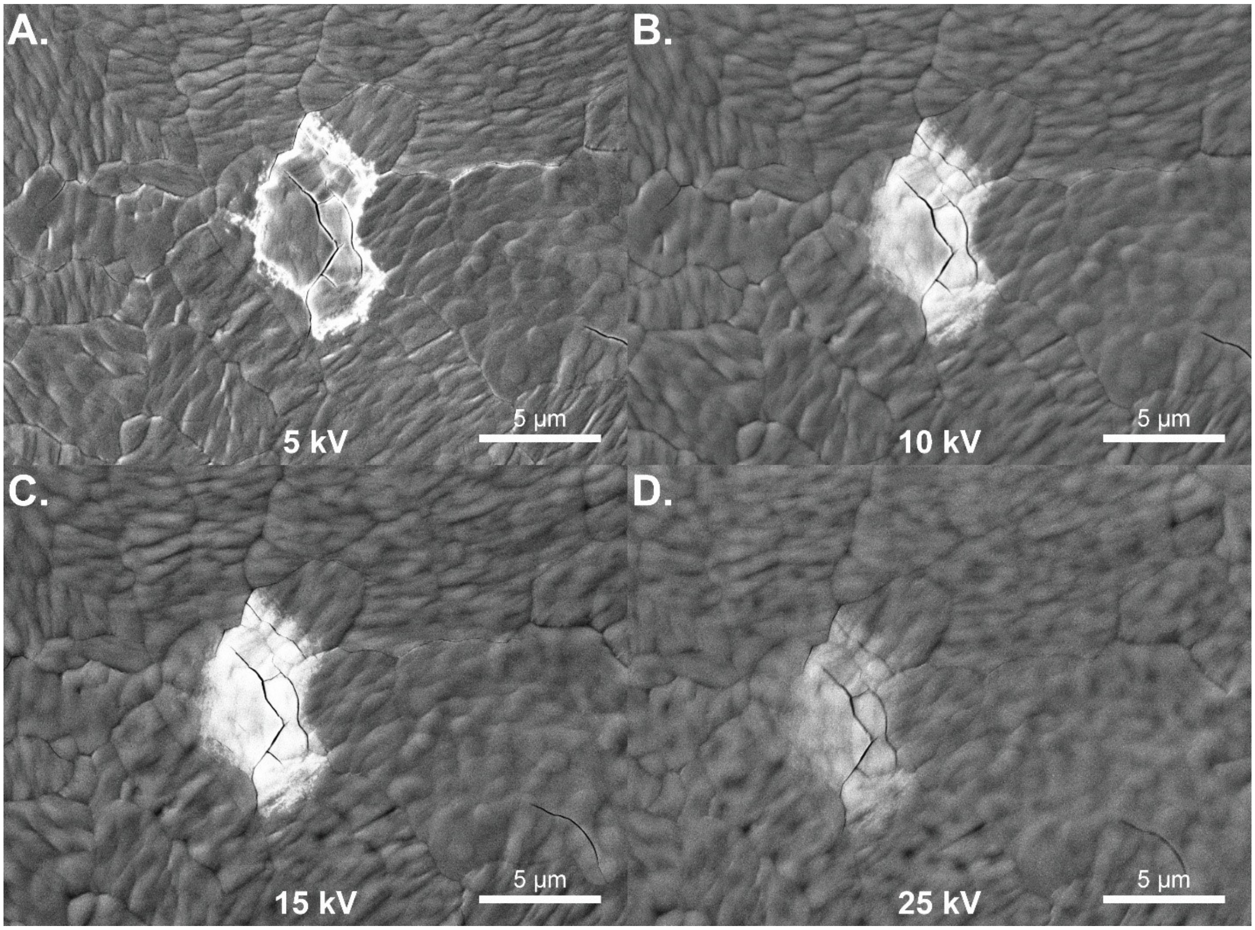

Figure S5. Imaging of δ-$CsPbI_3$ region with high voltage electron beam. SEM images of a δ-$CsPbI_3$ region using a primary electron beam energy, E_{PE}, of (A) 5 kV, (B) 10 kV, (C) 15 kV, and (D) 25 kV. In all images the probe current was set to a value of 6.

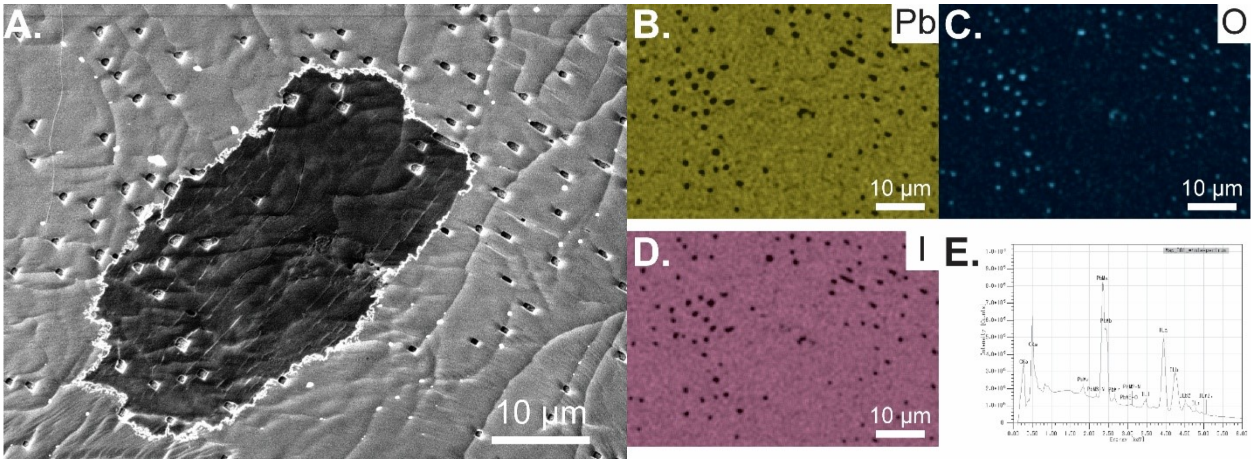

Figure S6. Extended compositional analysis of δ-$CsPbI_3$ region 1. (A) Secondary electron image (reproduced from **Figure 2A** of the main text) of a δ-$CsPbI_3$ region (dark) in a γ-$CsPbI_3$ film (E_{PE} = 2.3 kV, probe current = 40). EDS maps of this same location (E_{PE} = 8 kV) are shown for the (B) Pb, (C) O, and (D) I peaks of the spectrum. The full spectrum for the image in (A) is shown in (E). A small anomaly is seen in the center of the secondary electron image as well as the backscatter electron image. This corresponds to an elevated concentration of the carbon and oxygen in the EDS maps.

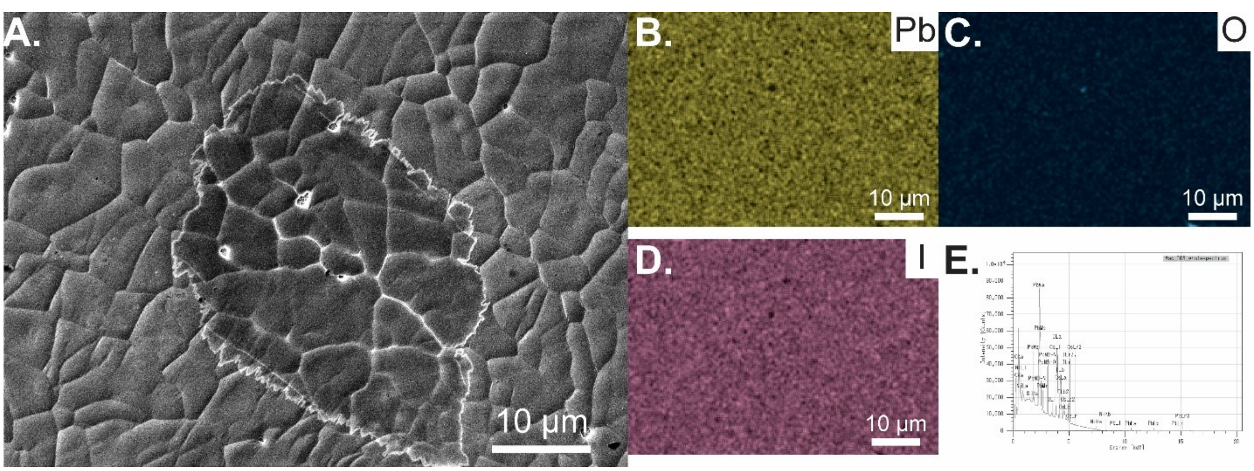

Figure S7. Extended compositional analysis of δ-$CsPbI_3$ region 2. (A) Secondary electron image (reproduced from **Figure 2D** of the main text) of a δ-$CsPbI_3$ region (dark) in a γ-$CsPbI_3$ film (E_{PE} = 3 kV, probe current = 30). EDS maps of this same location (E_{PE} = 8 kV) are shown for the (B) lead, (C) oxygen, and (D) iodine peaks of the spectrum. The full spectrum for the image in (A) is shown in (E). A small anomaly is seen in the center of the secondary electron image as well as the backscatter electron image, but is not clearly visible in the EDS maps.

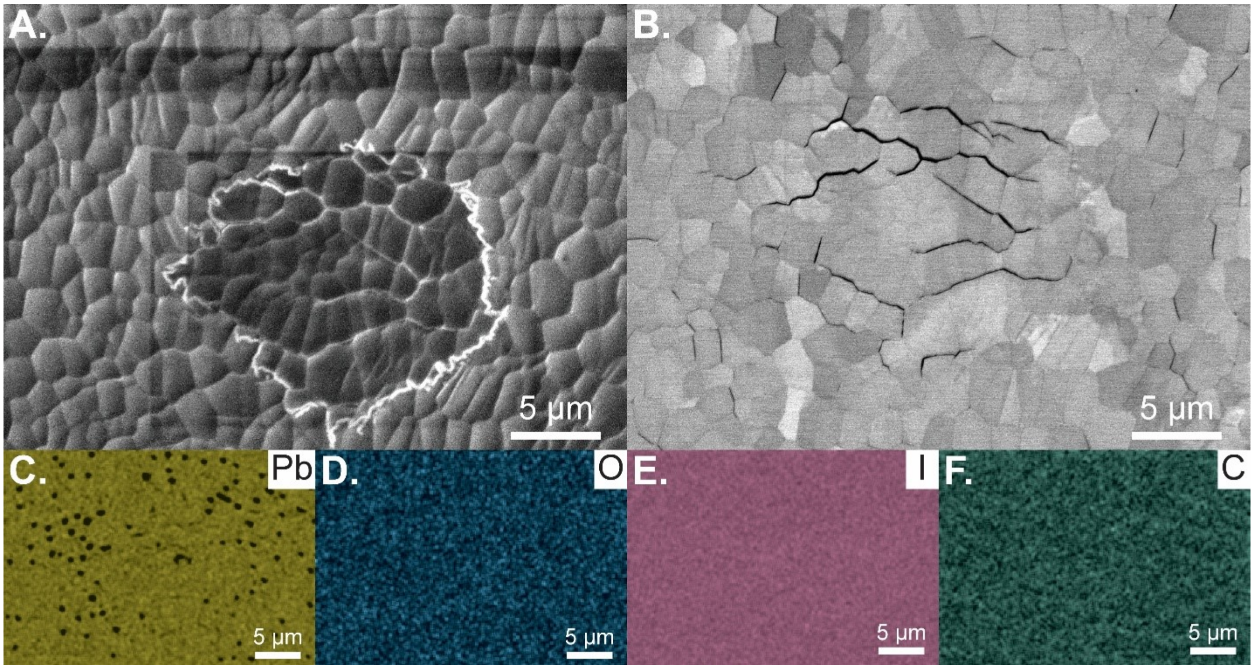

Figure S8. Analysis of δ-$CsPbI_3$ region 3. (A) Secondary electron image and (B) backscatter electron image of a δ-$CsPbI_3$ region (dark) in a γ-$CsPbI_3$ film (E_{PE} = 2.3 kV). EDS maps of this same location (E_{PE} = 8 kV) are show for the (C) lead, (D) oxygen, and (E) iodine, and (F) carbon peaks of the spectrum. No visible anomalies are clearly seen in this δ-$CsPbI_3$ region.

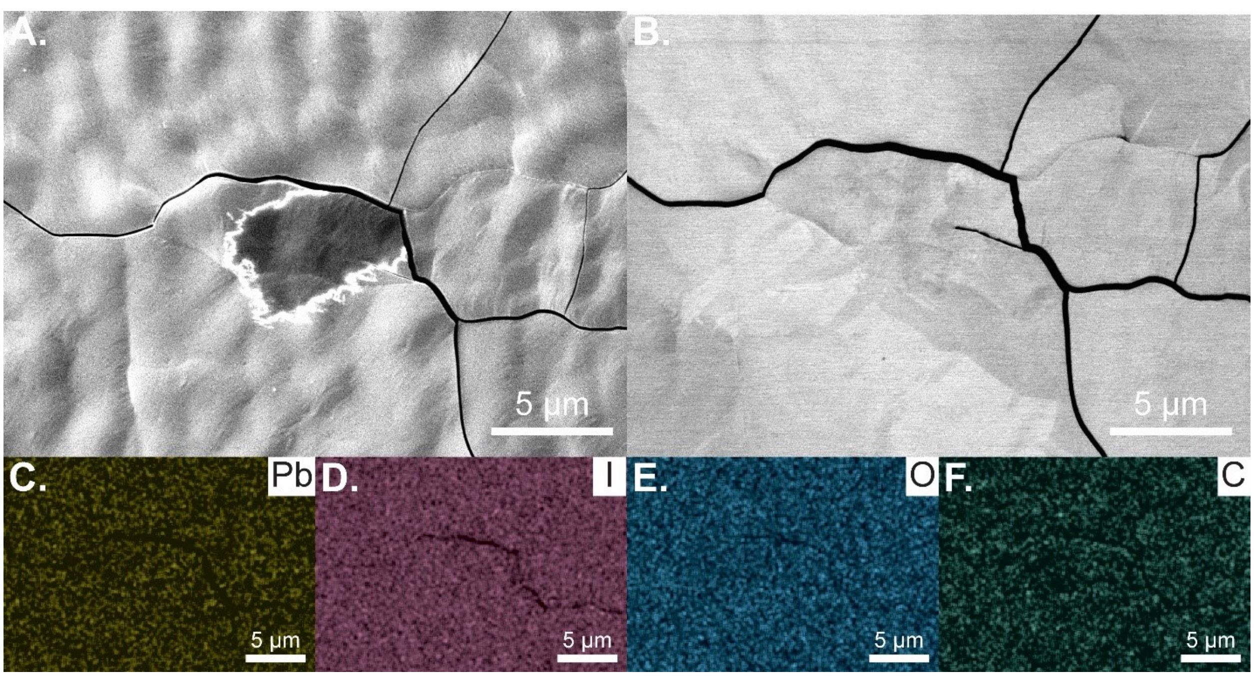

Figure S9. Analysis of δ-$CsPbI_3$ region 4. (A) Secondary electron image and (B) backscatter electron image of a δ-$CsPbI_3$ region (dark) in a γ-$CsPbI_3$ film (E_{PE} = 2.3 kV). EDS maps of this same location (E_{PE} = 8 kV)are show for the (C) lead, (D) iodine, (E) oxygen, and (F) carbon peaks of the spectrum. No visible anomalies are clearly seen in this δ-$CsPbI_3$ region.

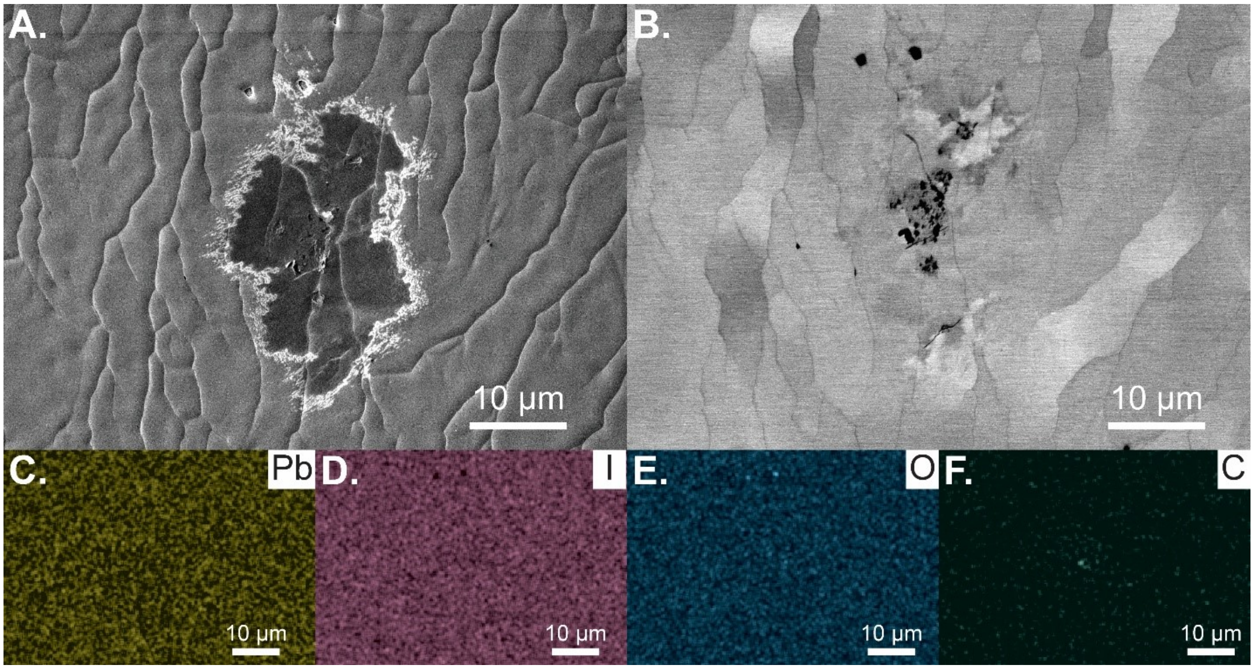

Figure S10. Analysis of δ-$CsPbI_3$ region 5. (A) Secondary electron image and (B) backscatter electron image of a δ-$CsPbI_3$ region (dark) in a γ-$CsPbI_3$ film (E_{PE} = 2.3 kV). EDS maps of this same location (E_{PE} = 8 kV)are show for the (C) lead, (D) iodine, (E) oxygen, and (F) carbon peaks of the spectrum. An anomaly is seen in the center of the secondary electron image as well as the backscatter electron image which corresponds to an increase in the carbon signal in EDS.

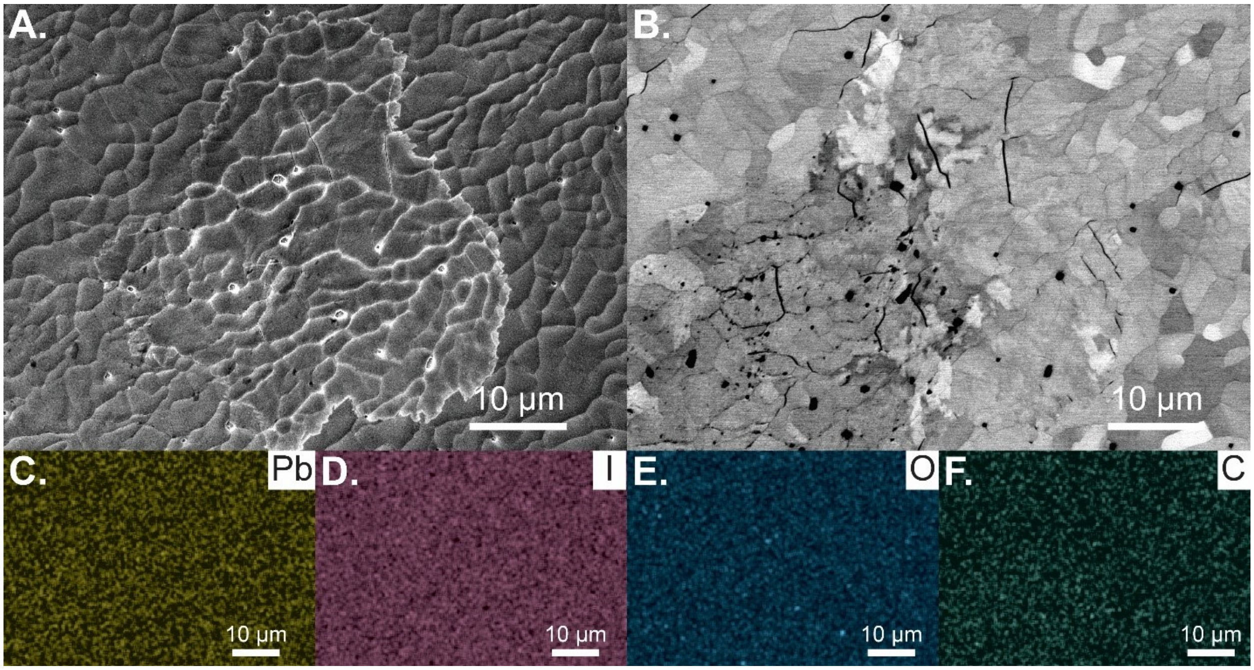

Figure S11. Analysis of δ-$CsPbI_3$ region 6. (A) Secondary electron image and (B) backscatter electron image of a δ-$CsPbI_3$ region (dark) in a γ-$CsPbI_3$ film(E_{PE} = 3 kV). EDS maps of this same location (E_{PE} = 8 kV) are show for the (C) lead, (D) iodine, (E) oxygen, and (F) carbon peaks of the spectrum. An anomaly is seen in the secondary electron image as well as the backscatter electron image, but is not clearly visible in the EDS maps.

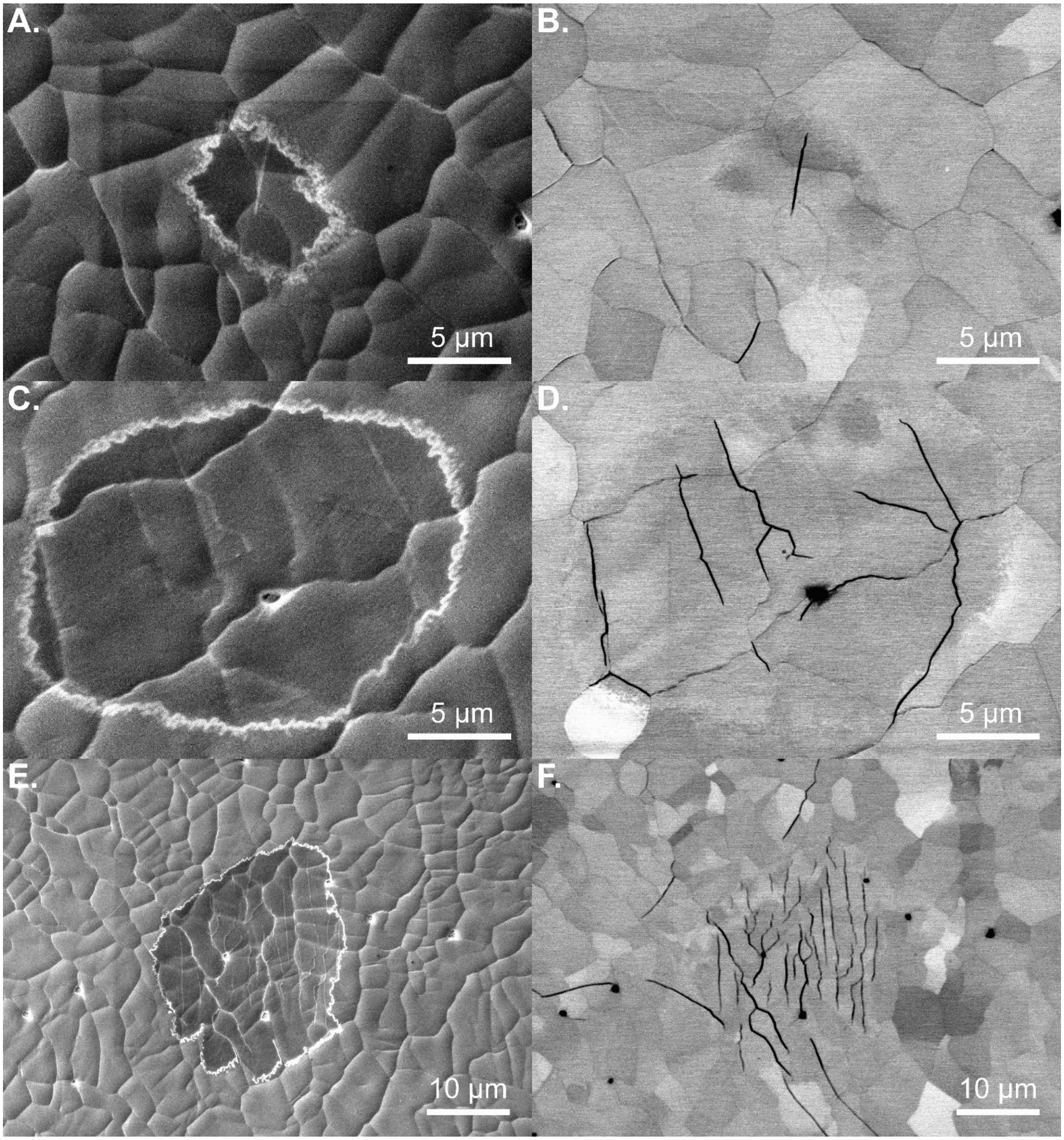

Figure S12. Analysis of δ-$CsPbI_3$ region 7-9. Secondary electron images (A, C, & E) and backscatter electron (B, D, & F) images of three different δ-$CsPbI_3$ region (dark) in a γ-$CsPbI_3$ film. A slight anomaly is seen in regions shown in the middle two images while nothing is clearly visible in the top or bottom region.

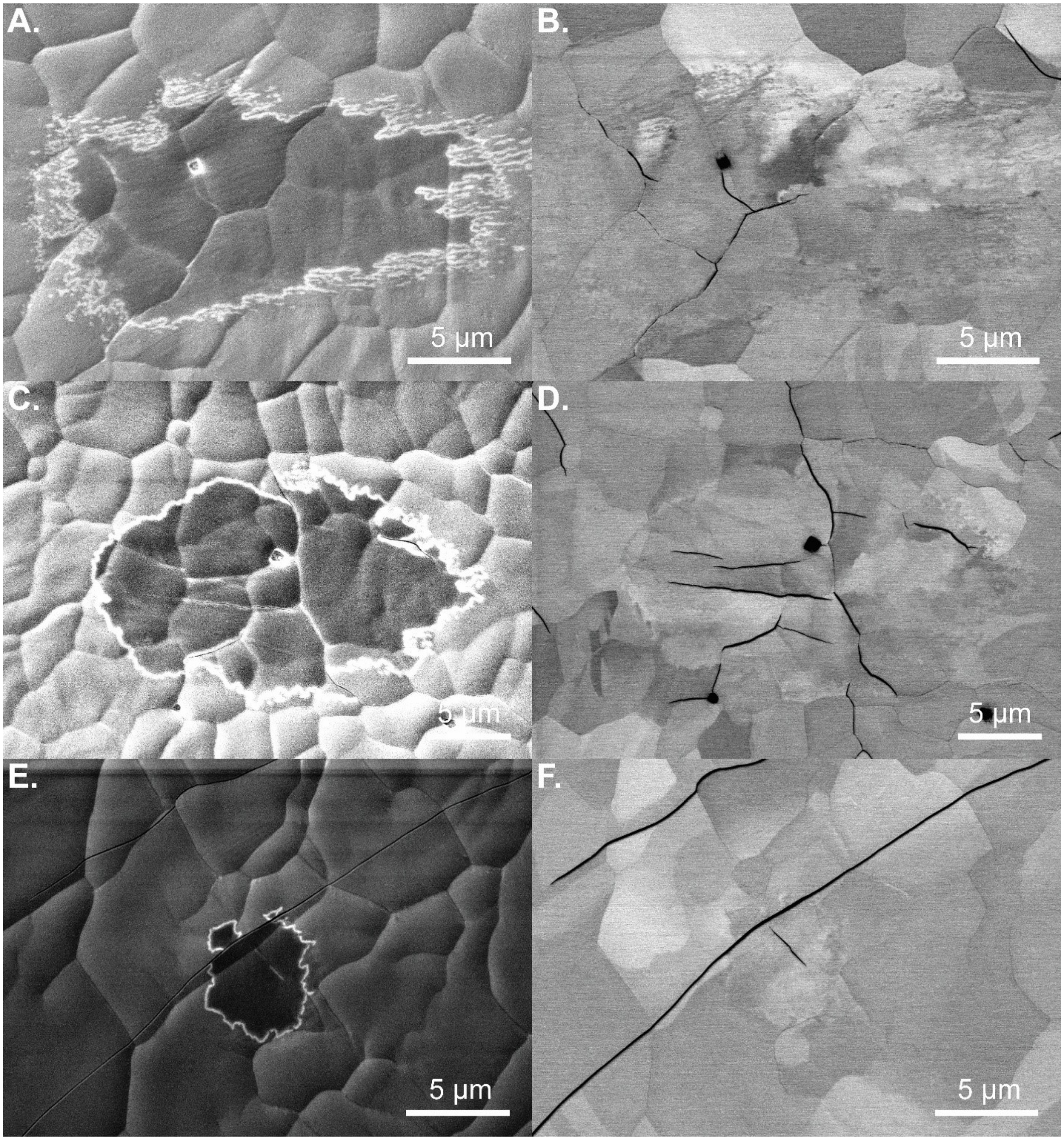

Figure S13. Analysis of δ-$CsPbI_3$ region 10-12. Secondary electron images (A, C, & E) and backscatter electron (B, D, & F) images of three different δ-$CsPbI_3$ region (dark) in a γ-$CsPbI_3$ film. All three regions show no clear sign of contamination or an anomaly in the δ-$CsPbI_3$ region.

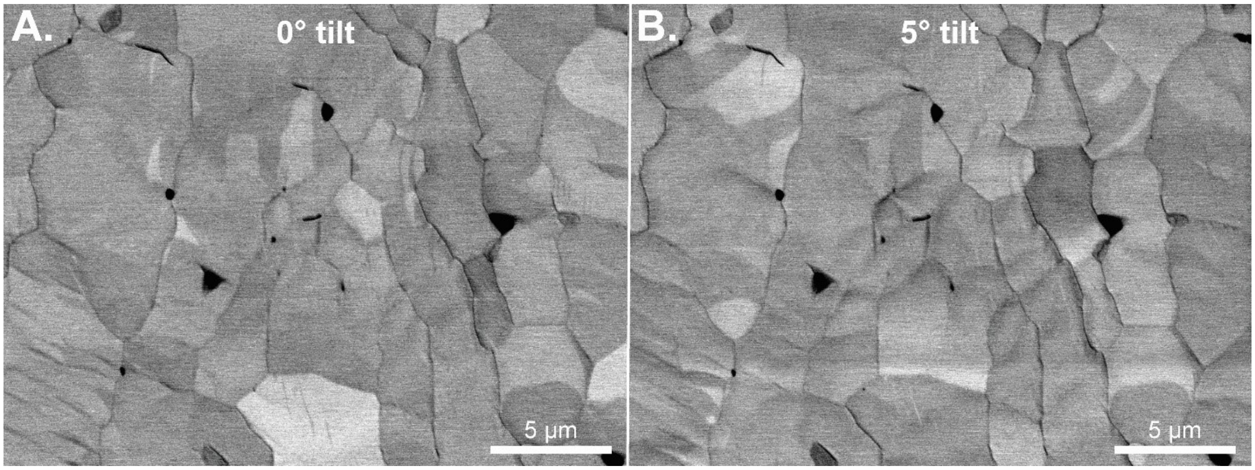

Figure S14. Backscatter electron imaging contrast with sample tilt. Images of the same location in a γ-$CsPbI_3$ film where the contrast primarily arises from electron beam channeling. In image (A) the sample is perpendicular to the incident electron beam while in (B) it is tilted at an angle of 5° off perpendicular. In both images E_{PE} is 3 kV and the probe current is set to 75.

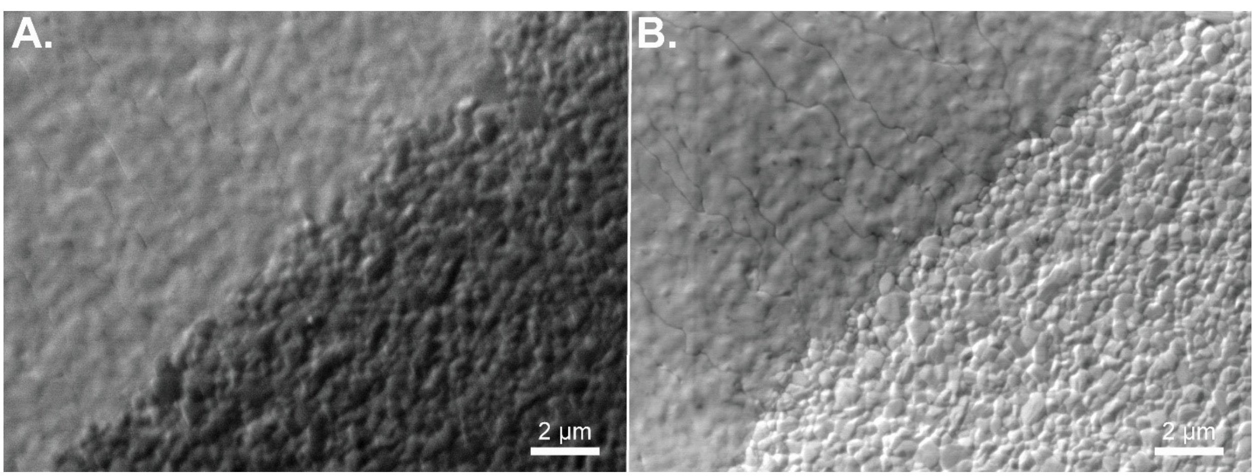

Figure S15. Contrast flip in $FAPbI_3$. (A) A typical image of a δ-$FAPbI_3$ region in a α-$FAPbI_3$ film with a probe current setting of 60 and E_{PE} set to 1.5 kV. The δ-$FAPbI_3$ region is lighter and the α-$FAPbI_3$ region is darker. (B) The contrast reverses when the probe current is increased to a setting of 90 so that the δ-$FAPbI_3$ region is darker and the α-$FAPbI_3$ region becomes lighter.